A Folate Receptor-Targeting Nanoparticle Minimizes Drug Resistance in a Human Cancer Model

Xu Wang,[†] Jun Li,[‡] Yuxiang Wang,[†] Lydia Koenig,[†] Ada Gjyrezi,[§] Paraskevi Giannakakou,[§] Edwin H. Shin,[⊥] Mourad Tighiouart,[∥] Zhuo (Georgia) Chen,[†] Shuming Nie,[‡] and Dong M. Shin[†,*]

[†]Department of Hematology and Medical Oncology, Winship Cancer Institute, and [‡]Department of Biomedical Engineering, Emory University School of Medicine, Atlanta, Georgia, United States, [§]Department of Pharmacology, Weill Medical College of Cornell University, New York, New York, United States, [⊥]Franklin College of Art and Science, University of Georgia, Athens, Georgia, United States, and [∥]Department of Biostatistics & Bioinformatics, Winship Cancer Institute, Emory University Rollins School of Public Health, Atlanta, Georgia, United States

ABSTRACT Resistance to chemotherapy is a major obstacle in cancer therapy. The main purpose of this study is to evaluate the potential of a folate receptor-targeting nanoparticle to overcome/minimize drug resistance and to explore the underlying mechanisms. This is accomplished with enhanced cellular accumulation and retention of paclitaxel (one of the most effective anticancer drugs in use today and a well-known P-glycoprotein (P-gp) substrate) in a P-gp-overexpressing cancer model. The folate receptor-targeted nanoparticle, HFT-T, consists of a heparin-folate-paclitaxel (HFT) backbone with an additional paclitaxel (T) loaded in its hydrophobic core. *In vitro* analyses demonstrated that the HFT-T nanoparticle was superior to free paclitaxel or nontargeted nanoparticle (HT-T) in inhibiting proliferation of P-gp-overexpressing cancer cells (KB-8-5), partially due to its enhanced uptake and prolonged intracellular retention. In a subcutaneous KB-8-5 xenograft model, HFT-T administration enhanced the specific delivery of paclitaxel into tumor tissues and remarkably prolonged retention within tumor tissues. Importantly, HFT-T treatment markedly retarded tumor growth in a xenograft model of resistant human squamous cancer. Immunohistochemical analysis further indicated that increased *in vivo* efficacy of HFT-T nanoparticles was associated with a higher degree of microtubule stabilization, mitotic arrest, antiangiogenic activity, and inhibition of cell proliferation. These findings suggest that when the paclitaxel was delivered as an HFT-T nanoparticle, the drug is better retained within the P-gp-overexpressing cells than the free form of paclitaxel. These results indicated that the targeted HFT-T nanoparticle may be promising in minimizing P-gp related drug resistance and enhancing therapeutic efficacy compared with the free form of paclitaxel.

KEYWORDS: targeting nanoparticle · paclitaxel · folate receptor · drug resistance · chemotherapy

The clinical success of paclitaxel with its broad anticancer spectrum has solidified the disruption of microtubule dynamics as one of the most effective anticancer strategies in use today. However, the emergence of drug-resistant cancer cells together with the toxicity of paclitaxel has greatly limited its clinical efficacy. P-glycoprotein (P-gp)-mediated resistance[1,2] has been described as one mechanism underlying multidrug resistance (MDR). P-gp, a product of the MDR1 gene, is a 170 kD transmembrane glycoprotein that functions as an efflux pump to remove drug from cells, thus reducing the intracellular concentration of the drug. Overexpression of the membrane-associated P-gp results in resistance to paclitaxel and other chemotherapeutic drugs.[3] This type of resistance is observed in many cancer types. To date, a large number of P-gp inhibitors have been investigated as potential anticancer agents. In preclinical studies, some of these P-gp inhibitors have shown the restoration of cancer cell sensitivity to anticancer drugs. Unfortunately, clinical trials of P-gp inhibitors have been disappointing due to suboptimal efficacy and their high toxicity.[4,5]

In light of this difficulty, nanotechnology, using nanoscaled drug delivery systems such as nanoparticles, polymeric-micelles, and lipsomes, offers an alternative strategy to address the drug resistance issue.[6−16] The mechanisms that underlie the MDR-reversal activities of nanoparticles are diverse and probably vary from one drug carrier to another, but include bypass drug-efflux pump resulting in increased cellular accumulation of the drug,[6,17] partial inhibition of P-gp function[18] and gene expression,[19] and modification of caspase-dependent apoptosis signaling pathways.[20] Recently we developed a novel targeted nanoparticle (HFT-T) that consists of a heparin-folate-paclitaxel (HFT) conjugate loaded with paclitaxel in its hydrophobic core for the specific delivery of paclitaxel to cancer cells overexpressing folate receptor (FR).[21] In an experimental model of human epidermal carcinoma (KB-3-1), HFT-T demonstrated strong therapeutic efficacy significantly superior to that of free paclitaxel and

* Address correspondence to dmshin@emory.edu.

Received for review February 23, 2011 and accepted July 5, 2011.

Published online July 05, 2011
10.1021/nn200739q

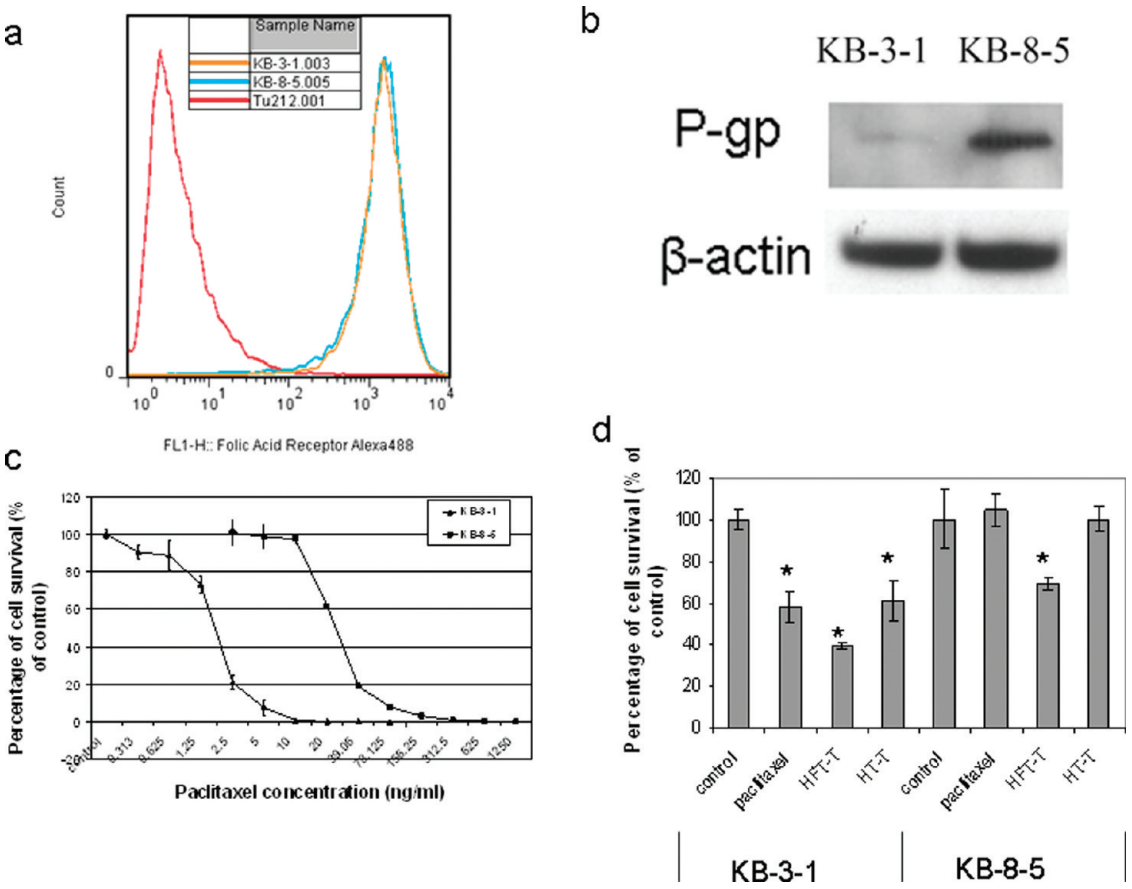

Figure 1. Cytotoxicity of HFT-T in drug-sensitive and -resistant cells. (a) Folic acid receptor expression on KB-3-1 and KB-8-5 cells. FR was overexpressed on both KB-3-1 and KB-8-5 cells when compared with FR-negative Tu212 cells. (b) P-gp expression on KB-3-1 and KB-8-5 cells. (c) Growth inhibition effect of paclitaxel in KB-3-1 and KB-8-5 cells. The IC_{50} of paclitaxel in KB-8-5 cells was 13-fold higher than that in KB-3-1 cells. (d) Cytotoxicity of HFT-T in KB-3-1 and KB-8-5 cells. Cells were incubated in 50 ng/mL free paclitaxel or HFT-T or HT-T (paclitaxel-equivalent dose for nanoparticles) for one hour, followed by incubation in drug-free medium for 48 h. (*p < 0.05 compared with control, results are mean ± SE).

nontargeted nanoparticles. The objectives of this study were to evaluate the potential of using the HFT-T nanoparticle in minimizing P-gp-mediated drug resistance and to explore the underlying mechanisms. We demonstrated that HFT-T is capable of increasing the intracellular accumulation of paclitaxel in drug-resistant epidermal carcinoma cells, which may be attributed to the failure of P-gp to mediate the efflux of nanoparticles. Importantly, HFT-T treatment markedly retarded the *in vivo* growth of drug-resistant tumors in animal models, indicating that HFT-T could be attractive in overcoming drug resistance and enhancing therapeutic efficacy clinically.

RESULTS AND DISCUSSION

Synthesis and Characterization of HFT-T Nanoparticles. The HFT-T nanoparticle was prepared as described in the Methods section.[21] First, the ternary conjugate heparin−folic acid−paclitaxel (HFT) was synthesized. Paclitaxel was conjugated onto the heparin backbone through the ester linker to yield HT; then ethylene diamine-modified folic acid was conjugated onto heparin through the amide linker to yield HFT. Second, free paclitaxel was incorporated into the HFT conjugates to form the HFT-T nanostructure by a self-assembly procedure with an efficiency of ≥90%. The content of paclitaxel in HFT-T was determined to be 26% (w/w). Suppl. Figure 1 shows the characterization of the HFT-T nanoparticle. The monodisperse shape of the HFT-T nanoparticle was clearly observed by transmission electron microscopy (TEM) negative staining (Suppl. Figure 1a). Dynamic light scattering (DLS) indicated the hydrodynamic size of the HFT-T nanoparticle was 60 ± 10 nm (Suppl. Figure 1b) and the zeta potential was −16.1 ± 1.1 mV. We also examined the controlled release kinetics of paclitaxel from the HFT-T nanoparticle, an important property for drug delivery. As shown in Suppl. Figure 1c, 33.1 ± 5.1% of the total paclitaxel was found to be released from the HFT-T nanoparticle during a 10-day dialysis in PBS buffer, indicating a slow release pattern of paclitaxel from HFT-T under physiological conditions. Since heparin was used to synthesize HFT-T, we determined the anticoagulant activity of the HFT-T nanoparticle, which was 0.23 ± 0.08 IU/mg and only accounted for 0.13% of that of unconjugated heparin (178 IU/mg).

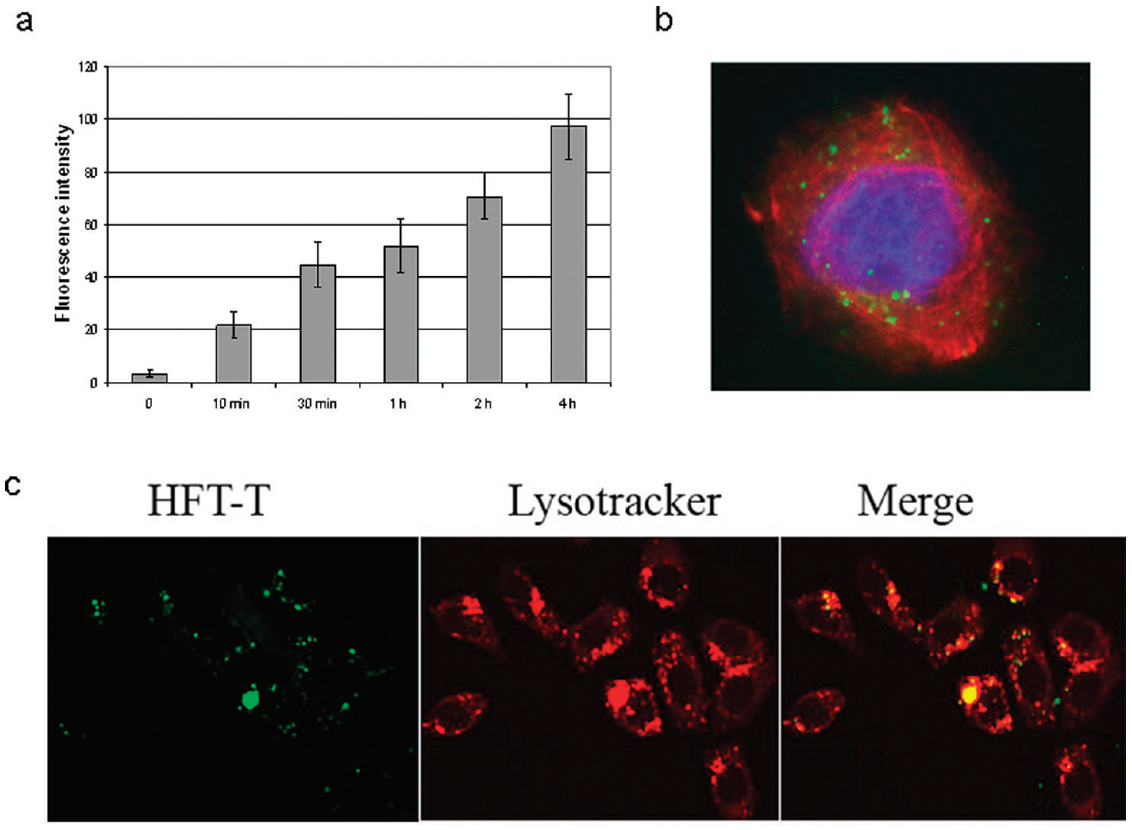

Figure 2. Cellular uptake of HFT-T in KB-8-5 cells. (a) Uptake of Oregon Green 488-labeled HFT-T by KB-8-5 cells at different time points was evaluated by FACS analysis. KB-8-5 cells were incubated with 0.2 μg/mL of Oregon Green 488-labeled HFT-T for 10 min, 30 min, 1 h, 2 h, and 4 h and analyzed using FACS. (b) Confocal images show KB-8-5 cell uptake of HFT-T labeled with Oregeon Green 488 after 1 h incubation. (c) Live cell images show uptake of labeled HFT-T by KB-8-5 cells 2 h after incubation. HFT-T is in green, and LysoTracker Red, detecting endosomes and lysosomes, is shown in red. Overlay between HFT-T and endosomes/lysosomes is represented in yellow.

HFT-T Nanoparticles Effectively Reduce Viability in Both Drug-Sensitive and Drug-Resistant Cancer Cells. The KB-8-5 human squamous cancer cell line, derived from paclitaxel-sensitive KB-3-1 cells, is a clinically relevant model that has been widely used in the study of drug resistance.[22,23] As shown in Figure 1a, both KB-3-1 and KB-8-5 cell lines express membrane-bound folic acid receptor, the potential target of the HFT-T nanoparticle. In contrast, only KB-8-5 cells substantially express the classical MDR marker P-glycoprotein (Figure 1b), which is consistent with their acquired MDR phenotype.

To compare the response of KB-3-1 and KB-8-5 cells to paclitaxel treatment, the cancer cells were exposed to a series of paclitaxel concentrations for 72 h, and then the cell growth inhibition effect of paclitaxel was analyzed. Indeed, upon treatment with paclitaxel, KB-8-5 cells exhibited a significantly higher resistance when compared to their drug-sensitive parental KB-3-1 cells, with an IC_{50} of 24 $\pm$ 5.61 ng/mL in KB-8-5 cells *versus* 1.8 $\pm$ 0.79 ng/mL in KB-3-1 cells (Figure 1c).

To compare the *in vitro* cytotoxicity of HFT-T nanoparticle in these drug-sensitive and -resistant cancer cells, drugs were added at 50 ng/mL final concentration (paclitaxel-equivalent dose for nanoparticle) for one hour; then the cells were washed three times with PBS to remove drugs and incubated in drug-free medium for 48 h.[15] Although all three paclitaxel formulations, *i.e*, free paclitaxel, HFT-T, and the nontargeting HT-T nanoparticles, reduced KB-3-1 cell viability to different degrees (60.5 $\pm$ 1.5%, 38.7 $\pm$ 9.7%, and 41.8 $\pm$ 7.5%, respectively), HFT-T exhibited the highest cytotoxicity in these chemosensitive cells, which was consistent with our previous observations.[21] Intriguingly, in KB-8-5 cells, only treatment with HFT-T resulted in a significant inhibition of cell survival (31.6 $\pm$ 2.9%), whereas free paclitaxel or HT-T did not markedly affect cell viability when added at the equivalent concentrations of HFT-T. These results indicated that the targeting HFT-T nanoparticle is more effective in reducing viability in both drug-sensitive and -resistant cancer cells, supporting its potential use to minimize drug resistance (Figure 1d).

Cellular Uptake, Retention, and Efflux of HFT-T Nanoparticle. We previously demonstrated that HFT-T displayed preferentially targeted binding and internalization in FR-expressing drug-sensitive cancer cells.[21] To further investigate the mechanisms for the enhanced *in vitro* cytotoxicity of HFT-T in KB-8-5 cells and the interaction between HFT-T and its targeted drug-resistant tumor cells, we evaluated the cellular uptake and efflux of

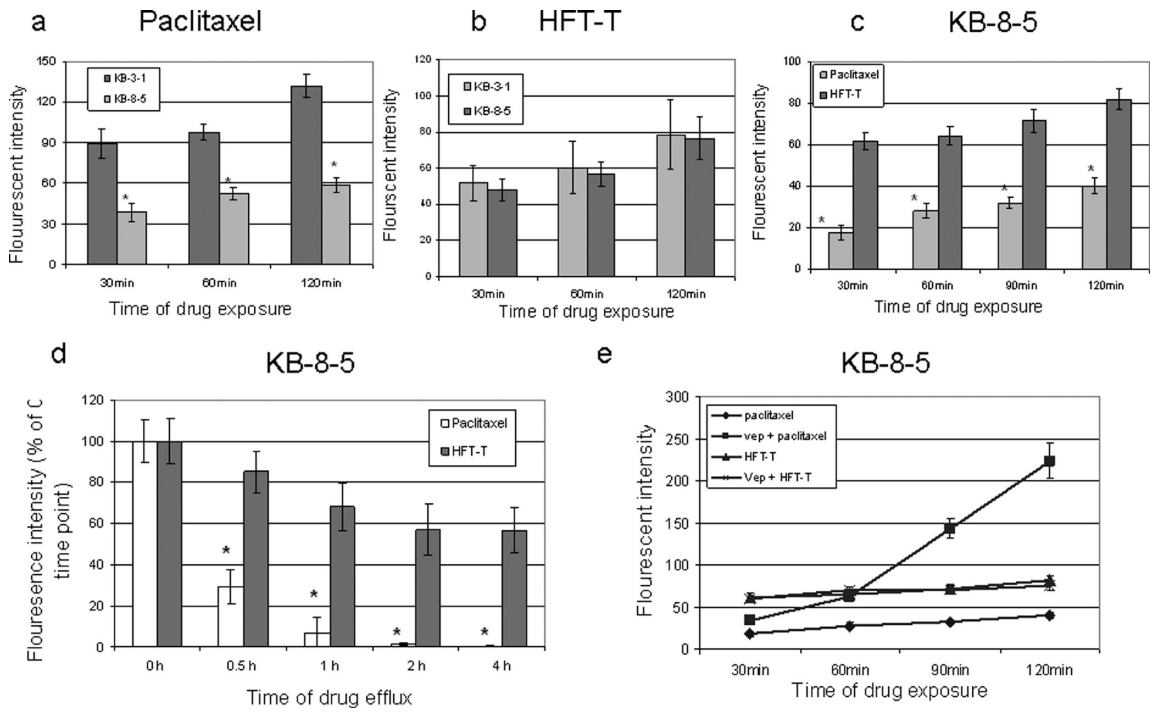

Figure 3. Cellular uptake and efflux of HFT-T in KB-3-1 and KB-8-5 cells. (a) Cellular uptake of free paclitaxel by KB-3-1 cells and KB-8-5 cells (*$p < 0.05$ compared with KB-3-1 cells at the same time point; results are mean ± SE). (b) Cellular uptake of HFT-T by KB-3-1 cells and KB-8-5 cells. (c) Cellular uptake of free paclitaxel and HFT-T by KB-8-5 cells (*$p < 0.05$ compared with HFT-T treatment at the same time point; results are mean ± SE). (d) Efflux of free paclitaxel and HFT-T in KB-8-5 cells. Cells were incubated with Oregeon Green 488-labeled free paclitaxel or HFT-T for 1 h and then reincubated with fresh drug-free cell culture medium for the indicated times (*$p < 0.05$ compared with HFT-T treatment at the same time point; results are mean ± SE). (e) Cellular uptake of free paclitaxel and HFT-T in KB-8-5 cells with or without P-gp inhibitor, verapamil. Cells were incubated with fluorescent dye-labeled HFT-T (0.2 μg/mL, paclitaxel-equivalent dose) at 37 °C in the presence or absence of verapamil (15 μM verapamil added into the culture medium 2 h before adding paclitaxel or HFT-T). At different time points after incubation, cells were washed three times with PBS and analyzed by FACS.

HFT-T in KB-8-5 cells. KB-8-5 cells were incubated with 0.2 μg/mL of HFT-T labeled with paclitaxel-Oregon Green 488 for 10 min, 30 min, 1 h, 2 h, and 4 h and then analyzed using flow cytometry (Figure 2). The uptake of HFT-T by KB-8-5 cells increased in a time-dependent manner (Figure 2a). In a live-cell imaging, co-localization of LysoTracker with HFT-T demonstrated that the majority of HFT-T was localized in endosomes/lysosomes after 2 h of incubation, suggesting endocytosis as the most likely mechanism of HFT-T uptake (Figure 2c). This is consistent with our previous observation in KB-3-1 cells, suggesting that HFT-T may also undergo FR-mediated internalization in KB-8-5 cells.[21] To further investigate the mechanism of cellular uptake in KB-8-5 cells, we detected FR subcellular location by immunofluorescent staining after cells were incubated with HFT-T, HT-T, or folic acid for 30 min. After incubation with HFT-T, confocal microscopy revealed internalization of FR from the cell membrane into the cell cytoplasm. A similar result was observed in folic acid-treated cells, but not in HT-T-treated cells. This behavior is consistent with a receptor-mediated endocytosis pathway for HFT-T internalization (Suppl. Figure 2).

The P-gp efflux pump is a major energy-dependent drug efflux mechanism that actively reduces the intracellular contents of cytotoxic agents. Since P-gp is highly overexpressed in many drug-resistant cancer cells,[3] we postulated this efflux pump may be responsible for the acquired resistance to paclitaxel in KB-8-5 cells. Indeed, comparison of the intracellular accumulation of paclitaxel found that the drug content in KB-8-5 cells was significantly lower (by ~50%) than that in KB-3-1 cells (Figure 3a). Interestingly, however, incubation of either KB-3-1 or KB-8-5 cells in the presence of HFT-T resulted in comparable levels of intracellular paclitaxel accumulation (Figure 3b), suggesting that the HFT-T formulation may counteract the transporter-mediated drug resistance in KB-8-5 cells, thereby increasing intracellular concentrations of paclitaxel and enhancing its cytotoxicity. In fact, compared to free paclitaxel, HFT-T was found to be capable of effectively delivering and maintaining markedly higher concentrations (by 2−3-fold) of paclitaxel in KB-8-5 cells when added to the cultures at varying times (Figure 3c).

We further questioned whether the high intracellular levels of paclitaxel delivered by HFT-T may be attributed, at least in part, to the insusceptibility of these nanoparticles to P-gp-mediated efflux in drug-resistant cancer cells. To perform the P-gp-mediated efflux assay, KB-8−5 cells were incubated with 0.2 μg/mL

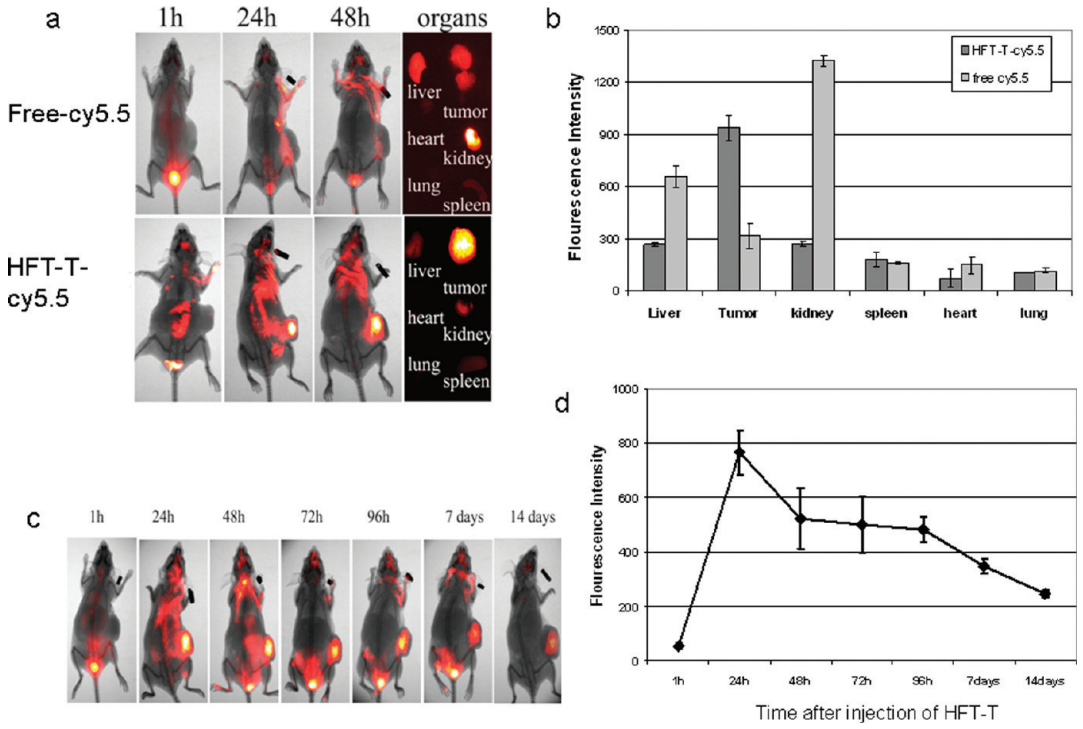

Figure 4. ***In vivo*** **distribution of HFT-T in KB-8-5 tumor-bearing mice. Near-infrared dye Cy5.5 or Cy5.5-labeled HFT-T was injected iv into KB-8-5 tumor-bearing mice. (a) Imaging of representative mice at 1, 24, and 48 h after injection. Imaging of representative major organs including liver, spleen, kidney, heart, lung, and tumors removed from mice 48 h after injection. For HFT-T-treated mice, the greatest fluorescence intensity was observed in the tumor compared with the other tissues. For free Cy5.5-treated mice, the greatest fluorescence intensity was observed in the kidney. (b) Fluorescence intensity in major organs at 48 h after injection of free Cy5.5 or HFT-T. (c) Tumor accumulation of Cy5.5-labeled HFT-T in KB-8-5 tumor-bearing mice. Imaging of representative mice at 1 h, 24 h, 48 h, 72 h, 7 days, and 14 days after injection. (d) Fluorescence intensity in tumors at indicated time points after injection of HFT-T. The background autofluorescence has been subtracted.**

Oregeon Green 488-labeled paclitaxel or HFT-T (paclitaxel-equivalent dose) for one hour at 37 °C and then washed three times with PBS to remove extracellular drug. The rinsed cells were incubated with drug-free medium at 37 °C for an additional 0.5, 1, 2, and 4 h and then analyzed by fluorescence-activated cell sorting (FACS) to measure the drug efflux. Figure 3d shows that in KB-8-5 cells incubated with free paclitaxel, only 30% of the paclitaxel was retained at 30 min and was completely removed within 2 h. In contrast, upon addition of HFT-T at an equivalent dose of free paclitaxel, the retention of paclitaxel in KB-8-5 cells was significantly increased, remaining at a high intracellular level of 56.7 $\pm$ 10.7% after 4 h (Figure 3d). These data indicate that HFT-T may not be susceptible to P-gp-mediated efflux. Supporting this notion, blockade of P-gp activity by verapamil, a P-gp inhibitor,[5] significantly increased the accumulation of free paclitaxel, but not HFT-T, in a time-dependent manner in KB-8-5 cells (Figure 3e).

These interesting data may explain the increased intracellular presence of paclitaxel in drug-resistant cancer cells when delivered by HFT-T nanoparticles. Despite its function as a major efflux pump for free drugs in MDR cancer cells, P-gp may fail to export paclitaxel when it is encapsulated within the HFT-T nanoparticle, which is consistent with reported studies.[6,17] This property of the HFT-T nanoparticle could result in the increased intracellular availability of paclitaxel, eventually contributing to the enhanced cytotoxicity of HFT-T in drug-resistant cancer cells.

In Vitro **Antiangiogenic Effect of HFT-T.** The HFT-T nanoparticle has a backbone primarily consisting of heparin, a natural polymer that could confer additional therapeutic advantages. Heparin has been associated with a better response to chemotherapy and prolonged survival in cancer patients,[24,25] which may be attributed to its tumor-inhibitory effects through binding growth factors and preventing their interaction with corresponding signaling receptors.[26−28] Heparin may also inhibit the activity of heparinase, which was thought to be required for tumor cells to invade the vascular basement membrane.[29,30] These observations allowed us to hypothesize that, in addition to the cytotoxicity mediated by encapsulated paclitaxel, the presence of heparin in the HFT-T formulation may also contribute to its antitumor activity. Indeed, by performing a tube formation assay using human umbilical vein endothelial cells (HUVECs), we demonstrated that both HFT-T and HT-T nanoparticles could significantly reduce the amount of tube formation, an indicator of inhibition of angiogenesis. On the contrary, there was

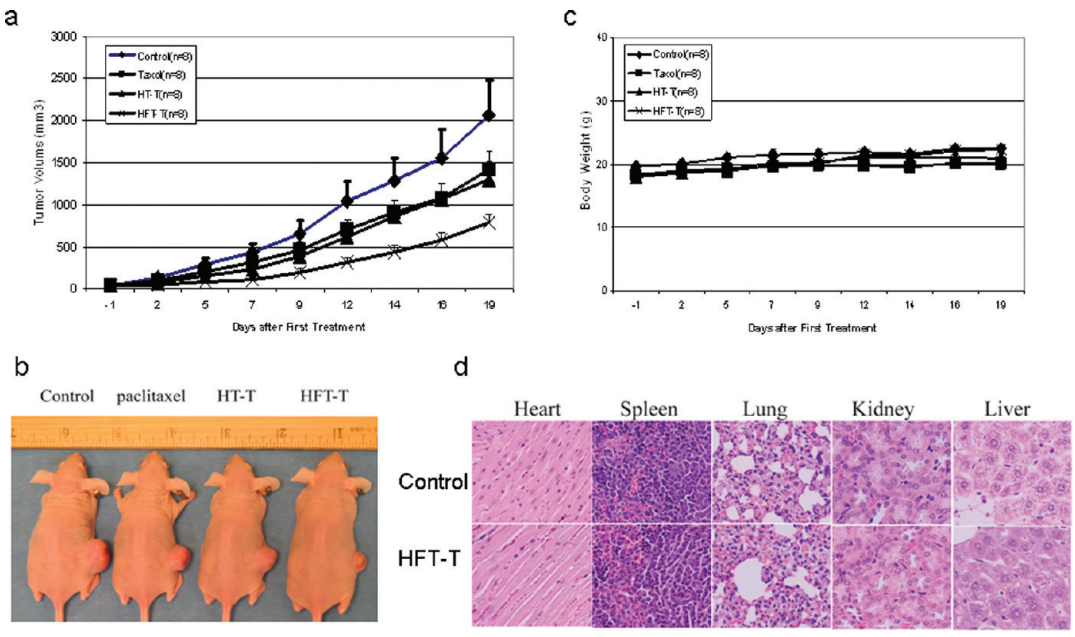

Figure 5. Antitumor effect of HFT-T nanoparticle in an animal model. (a) The tumor growth of KB-8-5 xenografts was significantly inhibited in the HFT-T-treated group compared with the control ($p = 0.0075$), free paclitaxel ($p = 0.0155$), and HT-T ($p = 0.0381$) treated groups. Tumor volumes in free paclitaxel ($p = 0.2287$) and HT-T ($p = 0.1423$) treated groups were not statistically significant different compared with the control group. On day 19, the average tumor volumes were as follows: 2061.7 ± 416.1 mm^3 for control, 1422.9 ± 216.1 mm^3 for paclitaxel, 1301.3 ± 213.9 mm^3 for HT-T, and 785.6 ± 104.1 mm^3 for HFT-T groups. (b) Representative mouse from each group. (c) Body weights of mice in all groups. The body weights of mice in all four groups were similar. (d) Representative images of H&E organ staining from control and HFT-T-treated mice (magnification 200×).

no significant difference in the amount of tube formation between the control and paclitaxel-treated groups. The average tube-forming scores were quantified as 4.84 ± 0.35 for the control, 3.5 ± 1.35 for paclitaxel, 2.8 ± 0.92 for HT-T, and 2.7 ± 0.67 for HFT-T (Suppl. Figure 3). These results indicate that the presence of heparin in the nanoparticles may be responsible for the observed antiangiogenic activity, which could contribute to the antitumor efficacy of HFT-T, and warrant further investigation into the underlying mechanisms.

***In Vivo* Accumulation of HFT-T in Xenograft Tumors.** One of the advantages of using targeted nanoparticles for drug delivery *in vivo* is that nanoparticles facilitate drug accumulation within tumors. To investigate the *in vivo* distribution of HFT-T compared with that of a small molecular agent (free Cy5.5), we prepared near-infrared dye (Cy5.5)-labeled nanoparticle HFT-T, which allowed real-time imaging of the *in vivo* distribution in mice bearing KB-8-5 tumors (Figure 4a). Following systemic injection through the tail vein, there was no intratumoral accumulation of either Cy5.5-labeled HFT-T or free Cy5.5 dye (control) at 1 h, but the fluorescence intensity was significantly increased within tumors in mice injected with HFT-T at 24 and 48 h. In contrast, at the same time points, no tumor accumulation of fluorescence was observed in mice injected with free dye. Free dye accumulated rapidly and continually remained in the kidney and bladder within 1 to 48 h following injection. It is worth noting that the fluorescence signal could also be observed in the bladder between 1 and 48 h after HFT-T injection, which may result from certain small-molecule dyes cleaved from the nanoparticles and/or from the heparin–dye conjugates that were dissociated with HFT-Ts. At 48 h after the injection, the liver, kidney, lung, heart, and spleen were collected, and fluorescence intensities were analyzed by Kodak imaging station IS2000MM. In HFT-T-treated mice, the greatest fluorescence intensity was observed in the tumor compared with the other tissues. In Cy5.5-treated mice, the highest fluorescence intensity was observed in kidney. As shown in Figure 4b, the fluorescence intensity in tumors was 3 times higher in HFT-T-treated mice (939.8 ± 75.8) than in free Cy5.5-treated mice (316.5 ± 72.1). Collectively, the results indicate that the HFT-T nanoparticle facilitated the *in vivo* accumulation of Cy5.5 within tumors to greater levels than the small molecular agent (free dye).

We further evaluated the kinetics of HFT-T accumulation in tumors. As shown in Figure 4c,d, the intensity of Cy5.5-HFT-T was increased during the 24 h after the injection, remained at a high level until 72 h, and then slowly declined thereafter. Remarkably, tumor accumulation of HFT-T still remained detectable after 14 days post-injection. These results indicated that the HFT-T nanoparticle may have prolonged retention within tumor tissues, which could enhance the exposure of tumors to therapeutic agents.[31]

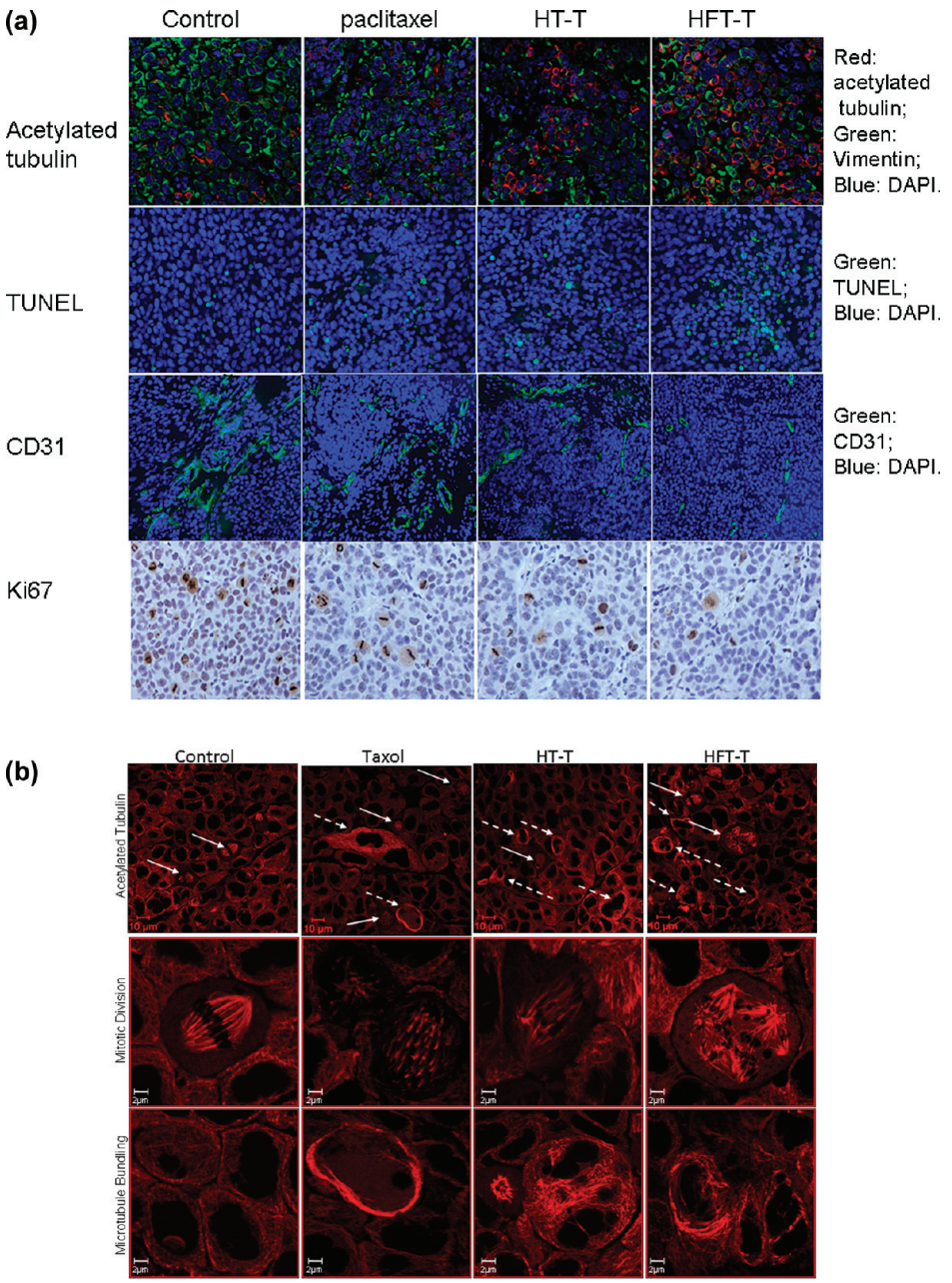

Figure 6. Effects of HFT-T on cell division, proliferation, and apoptosis. (a) Paraffin-embedded tissue sections from different treatment groups were immunostained with antiacetylated tubulin to detect acetylated tubulin, anti-KI-67 for cell proliferation, CD31 for angiogenesis, and TUNEL staining for the detection of apoptotic cells. Acetylated-α-tubulin in red; CD31 in green; apoptotic cells are shown in green; DNA counterstained with DAPI in blue (magnification 200×). (b) Arrows point to mitotic figures. Arrow in control: normal dividing cell in anaphase. Arrow in treatment groups: aberrant mitotic arrest. Dashed arrow: microtubule bundling.

***In Vivo* Antitumor Efficacy of HFT-T.** We evaluated the antitumor efficacy of HFT-T in KB-8-5 xenograft models. Tumor-bearing mice were randomly divided into four groups (n = 8): control group treated with PBS, free paclitaxel group (40 mg/kg paclitaxel), HT-T group (40 mg/kg paclitaxel-equivalent dose), and HFT-T group (40 mg/kg paclitaxel-equivalent dose). The treatment was administered once per week through tail vein injection and lasted for 3 weeks (injection time: days 1, 7, and 14). When the tumor sizes reached the maximum according to the Institutional Animal Care and Use Committee (IACUC) guidelines, the mice were sacrificed. A log−linear mixed model with random intercept was used to compare the mean tumor volumes between the treatment and control groups. The tumor volumes in the HFT-T-treated group were significantly reduced compared with all other treatment groups including the control (p = 0.0075), free paclitaxel (p = 0.0155), and HT-T (p = 0.0381) treated groups (Figure 5a). In contrast, tumor volumes in paclitaxel (p = 0.2287) and HT-T-treated (p = 0.1423) groups were not significantly different from the control group.

These results indicate that the therapeutic efficacy of the targeted HFT-T nanoparticle is significantly superior to that of free paclitaxel and nontargeted nanoparticle in drug-resistant xenograft models. Indeed, after three weeks of treatment (on day 19), the average tumor volumes (726.6 ± 104.1 mm^3) in the HFT-T-treated group were significantly smaller than in the free paclitaxel (1422.9 ± 216.1 mm^3; $p = 0.007$) or HT-T-treated (1301.3 ± 213.9 mm^3; $p = 0.012$) groups. Representative mice from each group are shown in Figure 5b. These results indicate that HFT-T is much more effective than free paclitaxel in treating drug-resistant tumors, which are a common occurrence in patients clinically treated with chemotherapeutic agents.

In the development of nanoparticles, an important consideration is their potential toxicity, especially during chronic administration. Heparin has been widely used as an injectable anticoagulant because of its intrinsic anticoagulation function. Since heparin was used to synthesize HFT-T, we evaluated the anticoagulant activity of HFT-T, which was determined as 0.23 ± 0.08 IU/mL, only 0.13% of that of unconjugated heparin (178 IU/mg). We further evaluated the systemic toxicity of free paclitaxel, HT-T, and HFT-T in the KB-8-5 xenograft model. Importantly, compared with the control group, the body weights of mice in all three treatment groups were similar, indicating a negligible acute toxicity at this dose (40 mg/kg paclitaxel-equivalent) (Figure 5c). This was further confirmed by histopathologic analyses of major organs (including liver, spleen, kidney, heart, and lung) from the mice sacrificed on day 19 (3-week treatment). No tissue damage was observed in any organ samples collected from any treatment group, including HFT-T (Figure 5d).

Folic acid (FA) was chosen as the targeting moiety in the HFT-T nanoparticle for its several advantages: low molecular weight and immunogenicity, relatively high stability, and ease of synthesis. Importantly, expression of folate receptor α is relatively low and highly restricted in normal tissues, including pancreas (duct epithelium), breast, lung (bronchial glands and pneumocytes), kidney, esophagus (glandular duct epithelium), parotid gland, and liver (bile ducts).[32,33] On the contrary, FR has been found to be highly expressed in a wide range of solid tumors, including ovarian, uterine, lung, breast, and head and neck cancers.[23,28] These properties make folate an excellent tumor-targeting moiety in the design of multifunctional nanoparticles.[34] It worth noting that although the accumulation of HFT-T in the liver and kidney was relatively high, no obvious tissue damage was observed in any of the organ samples collected from any treatment group, including HFT-T and HT-T. Several facts may account for the low acute *in vivo* toxicity of HFT-T under the tested conditions: (1) low FR expression in normal tissues when compared with that in tumors. Consistent with our findings, in a phase I clinical study, the FRα-targeted humanized monoclonal antibody (mAb) therapeutic agent farletuzumab was well tolerated in the management of heavily pretreated patients with epithelial ovarian cancer;[32] (2) the biodegradable heparin polymer may allow HFT-T accumulated in the liver and kidney to be readily degraded and subsequently eliminated through the renal system. Supporting this notion, we continually observed a fluorescence signal in the bladder after injection of fluorescent dye-labeled HFT-T, which may have resulted from the degradation and elimination of nanoparticles (Figure 4c); (3) a major mechanism of action of paclitaxel is to induce apoptosis in rapidly proliferating cells by stabilizing microtubules and interrupting mitotic division. Since the cell proliferation rate in normal adult liver and kidney tissues is very low compared with that in tumor tissues, it is plausible to postulate that HFT-T could exert its potent antitumor activity without significantly inducing tissue damage during a short-term treatment.

***In Vivo* Effect of HFT-T on Microtubules, Angiogenesis, Apoptosis, and Cell Proliferation in Xenograft Tumor Tissues.** A major mechanism of action of paclitaxel is to induce microtubule stabilization by tubulin acetylation. To determine if the enhanced antitumor activity of HFT-T *in vivo* correlated with the effect of HFT-T on microtubules in the cancer cells, we examined the levels of acetylated α-tubulin in xenograft tumor tissues. Immunofluorescent staining of acetylated α-tubulin in the HFT-T-treated group demonstrated significantly increased positive staining (44.50 ± 7.71%) as compared with the control (25.55 ± 12.87%) ($p = 0.013$) (Figure 6a). In contrast, acetylated tubulin levels in paclitaxel- (30.76 ± 15.26%) or HT-T-treated (40.86 ± 18.53%) groups were not significantly different from those in the control group ($p = 0.262$ and $p = 0.061$, respectively) (Figure 6a). Furthermore, drug-induced stabilization of interphase microtubules, as evidenced by an increase in microtubule polymer mass resulting in bundling, was observed in the tumor tissues from all the treatment groups and was the most significant in HFT-T-treated tumors (Figure 6b). These data indicate that HFT-T may have a more profound effect on the stabilization of microtubules in tumors.

Finally we analyzed the *in vivo* effects of HFT-T treatment on tumor angiogenesis, apoptosis, and proliferation by immunohistochemical (IHC) staining. Figure 6a shows that although a decrease in CD31-positive tumor microvessels was observed upon treatment with free paclitaxel, HT-T, and HFT-T, HFT-T was most effective in preventing the formation of tumor vasculature. The average microvessel count (per 100× field) was significantly reduced in HFT-T-treated tumor tissue (19.08 ± 3.62) compared to control (39.38 ± 6.84; $p < 0.001$) and paclitaxel-treated tumor tissue (22.75 ± 4.05; $p = 0.015$). When compared to the control, treatment with HT-T (29.60 ± 6.27; $p = 0.007$) or paclitaxel

(22.75 ± 4.05; $p = 0.076$) only moderately reduced the microvessel count.

IHC analyses of K_i-67 showed a significantly reduced level of K_i-67 in HFT-T-treated tumors (weighted index of K_i-67: 0.682 ± 0.028) than in the control (1.01 ± 0.025; $p < 0.001$), paclitaxel (0.846 ± 0.028; $p < 0.001$), or HT-T-treated (0.797 ± 0.027; $p = 0.015$) groups (Figure 6a). TUNEL assay revealed a significant increase in apoptotic tumor cells in the tumor tissues from the HFT-T-treated group (0.051 ± 0.024) as compared with the control group (0.030 ± 0.018; $p = 0.003$). HT-T (0.040 ± 0.021) and paclitaxel (0.038 ± 0.019) treatment slightly increased the number of apoptotic cells as compared with the control, although the difference was not significant (Figure 6a). Taken together, these data indicate that HFT-T treatment was more efficacious in inducing microtubule stabilization, mitotic arrest, and inhibition of cell proliferation than the other tested treatments, which was consistent with the superior *in vivo* antitumor efficacy of HFT-T (Suppl. Figure 4).

In conclusion, our studies have demonstrated that a FR-targeted nanoparticle, HFT-T, could significantly increase the intracellular concentration and retention of paclitaxel by facilitating drug uptake and reducing the drug efflux rate in MDR cancer cells, which may contribute to the enhanced specificity of drug delivery and prolonged drug retention within tumors. Importantly, HFT-T markedly enhanced the antitumor efficacy of paclitaxel in a drug-resistant KB-8-5 xenograft model. These results indicate that targeted nanoparticles could be a specific and efficient drug delivery system to overcome P-gp-mediated drug resistance in human cancer.

MATERIALS AND METHODS

Tumor Cell Lines and Cell Culture. The FR-overexpressing human epidermal carcinoma cell lines KB-3-1 and KB-8-5 were generously provided by Dr. Michael M. Gottesman (NCI, NIH, Bethesda, MD) and have been previously characterized.[35] KB-3-1 is a drug-sensitive cell line and KB-8-5 is a drug-resistant cell line that overexpresses P-glycoprotein.[36] KB-3-1 cells were maintained in DMEM medium supplemented with 10% fetal bovine serum (FBS). KB-8-5 cells were maintained in 10% FBS DMEM medium containing 10 ng/mL colchicine.

Preparation and Characterization of Nanoparticles. FR-targeted and nontargeted nanoparticles HFT-T and HT-T were prepared and characterized as previously described.[21] Briefly, in order to obtain the targeted nanoparticles, heparin bearing paclitaxel and folic acid in the side-chains (HFT) was synthesized first. Using the same process, paclitaxel only (without folic acid) was chemically conjugated onto heparin to yield the HT conjugate. To prepare the drug-loaded nanoparticles (HFT-T and HT-T), polymer HFT or HT (100 mg, paclitaxel content: 15% w/w) and free paclitaxel (15 mg) were dissolved in DMSO (3 mL). The solution was added into $NaHCO_3$ (0.1 M, 20 mL) dropwise. DMSO was removed by dialysis. The resulting solution was filtered using a 0.2 μm membrane and concentrated on an Ultra centrifugal filter (MW = 5000). The final content of paclitaxel in the stock solution of HFT-T was 26% (w/w), determined by UV absorption. Transmission electron microscopy showed that HFT-T nanoparticles were monodisperse (Suppl. Figure 1a). The dynamic size of the HFT-T nanoparticle was 60 ± 10 nm measured by a dynamic light scattering detector (Brookhaven Instruments, Holtsville, NY) (Suppl. Figure 1b). Since heparin was used to synthesize HFT-T, we determined the anticoagulant activity of HFT-T to be 0.23 ± 0.08 IU/mg, only 0.13% of unconjugated heparin (178 IU/mg). The detailed procedures regarding nanoparticle preparation and characterization are described in the Supporting Information.

The drug releasing from HFT-T nanoparticle was studied by dialyzing HFT-T in 10 L of PBS (pH 7.4) with gentle stirring at 37 °C to mimic physiological conditions. The amount of paclitaxel that remained in the nanoparticles at each release time point was measured by UV−vis spectroscopy in triplicate. The release of paclitaxel from HFT-T is shown in Suppl. Figure 1c.

Coagulation Assays. The anticoagulant activities of HFT-T were determined by the FXa-dependent coagulant assay using Coatest heparin according to the manufacturer's instructions. Briefly, 200 μL of heparin standard samples (concentrations of heparin from 0.01 to 0.07 unit/mL) and HFT-T were incubated at 37 °C for 3−4 min; then 100 μL of FXa (0.355nkat) was added and mixed well. The mixture was incubated at 37 °C for 30 s, and 200 μL of 1 mM of chromogenic substrate S-2222 was added. The mixture was incubated at 37 °C for 3 min. The reaction was stopped by adding 300 μL of 20% (v/v) acetic acid. The sample was transferred to a semimicro plate, and the absorbance of the samples at 405 nm was detected. The anticoagulant activity was calculated on the basis of the standard curve.[37]

Cell Growth Inhibition Assay. Cells were seeded at a density of 5×10^3 cells per well into 96-well plates in triplicate. Twenty-four hours later, paclitaxel was added at various concentrations (0.31−78.13 ng/mL for KB-3-1 cells, 2.5−1250 ng/mL for KB-8-5 cells) and continually incubated for 72 h. Cell growth inhibition was measured by determining cell density with the sulforhodamine B assay. The percentage of inhibition was determined by comparison of cell density in the drug-treated cells with that of the untreated control cells. All experiments were repeated three times.

***In Vitro* Cytotoxicity of HFT-T.** Cells were seeded at a density of 5×10^3 cells per well into 96-well plates in triplicate. Twenty-four hours later, drugs were added at 50 ng/mL final concentration (paclitaxel-equivalent dose for nanoparticles) for 1 h; then the cells were washed three times with PBS to remove drugs and incubated in drug-free medium for 48 h.[15] Cell growth inhibition was measured by determining cell density with the sulforhodamine B assay. The percentage of inhibition was determined by comparison of cell density in the drug-treated cells with that of the untreated control cells. All experiments were repeated at least three times.

Flow Cytometry Analysis. Flow cytometry analysis was used to evaluate the cellular uptake, retention, and efflux of fluorescent dye-labeled paclitaxel and HFT-T in the cells. Fluorescent dye-conjugated paclitaxel (paclitaxel−Oregon Green 488, Invitrogen, Carlsbad, CA) and fluorescent dye-labeled HFT-T were used to study drug accumulation in KB-3-1 and KB-8-5 cells. Fluorescent dye-labeled HFT-T or HT-T was prepared by encapsulation of paclitaxel−Oregon Green 488. KB-8-5 cells were seeded in six-well plates at 1×10^5 cells/well and allowed to attach overnight. Cells were incubated with paclitaxel−Oregon Green 488 or fluorescent dye-labeled HFT-T (0.2 μg/mL, paclitaxel-equivalent dose) at 37 °C in the presence or absence of verapamil (15 μM verapamil added into the culture medium 2 h before adding paclitaxel or HFT-T). At different time points after incubation, cells were washed three times with cold PBS, and then the cells were resuspended in 500 μL of PBS. The cell samples were analyzed using a fluorescence-activated cell sorting caliber benchtop flow cytometer (BD Biosciences). The drug accumulation data were analyzed using FlowJo software (Tree Star, Ashland, OR).

For the efflux study, cells were incubated with 0.2 μg/mL paclitaxel–Oregeon Green 488 or HFT-T (paclitaxel-equivalent dose) for 1 h at 37 °C and then washed three times with PBS, and the cells were then incubated with drug-free medium at 37 °C for another 0, 0.5, 1, 2, and 4 h. Cells were then washed three times with ice-cold PBS and analyzed by FACS. FlowJo software (Tree Star, Ashland, OR) was used for data analysis. All the experiments were repeated three times independently.

Capillary Tubule Formation Assay. A Matrigel-based capillary tube formation assay was performed using human umbilical vascular endothelial cells (Lonza Walkersville, MD). HUVECs were maintained in the endothelial cell basal medium-2 containing the following growth supplements: hydrocortisone, hFGf-B, VEGF, R3-IGF-1, ascorbic acid, heparin, FBS, hEGF, GA-1000; 4×10^4 cells/well were seeded on Matrigel (BD Bioscience, Bedford, MA)-coated 24-well plates and incubated at 37 °C for 18 h in a humidified 5% CO_2 atmosphere, in either the presence or absence of 0.1 ng/mL paclitaxel, equivalent dose of HFT-T, or HT-T. Each treatment was performed in triplicate. Tube formation was examined and scored under an inverted light microscope using 20× magnification.[38] On the basis of the quality and number of tubes, a score was assigned: 0, no real tubes; 1, some poorly formed tubes; 2, some formed tubes; 3, network of poorly formed tubes; 4, network of formed tubes; and 5, network of well-formed tubes. The experiment was repeated three times.

***In Vivo* Antitumor Efficacy Assay.** The animal experiment was approved by the Institutional Animal Care and Use Committee of Emory University. KB-8-5 cells (5×10^5) were injected sc into 4–5-week-old female nude mice (athymic *nu/nu*, Taconic, NY). When the tumors had developed to about 100 mm^3, the mice were divided into four groups ($n = 8$) in a way to minimize weight and tumor size differences among the groups: control group treated with saline, free paclitaxel group (40 mg/kg), HT-T group, and HFT-T group (40 mg/kg paclitaxel-equivalent for nanoparticles). Therapy was continued once per week through tail vein injection for three weeks (at day 1, 7, and 14). The body weight and tumor size were measured three times per week. The tumor volume was calculated using the formula $V = \pi/6 \times (\text{larger diameter}) \times (\text{smaller diameter})^2$. One week after the last treatment, tumor and organ tissues (liver, heart, lung, spleen, and kidney) were collected for H&E staining and immunostaining analyses.

Immunofluorescence, Immunohistochemistry, and TUNEL Assay. Immunofluorescence analysis of CD31 staining on frozen mouse xenograft tissue sections was performed. Tissue sections were incubated with rat anti-mouse CD31 primary antibody (BD Pharmingen) or rat IgG for control and Fluor-conjugated secondary antibodies. Slides were counterstained with DAPI (Vector Laboratories, Burlingame, CA). Images were taken with a Zeiss LSM510 META confocal microscope. Five images of the most intensively vascularized area were taken at 100× magnification for each slide stained for CD31. Microvessel density was examined by counting the numbers of microvessels in each image (×100 field). The result was presented as an average of numbers of microvessels per ×100 field.[39] Double staining for acetylated tubulin and vimentin was performed using paraffin-embedded mouse xenograft tissue as previously described.[21] The TUNEL assay was performed by immunofluorescence using the same specimens as above, following the procedure provided by the manufacturer (Promega, Madison, WI).

Immunohistochemical analysis for K_i-67 staining on paraffin-embedded mouse xenograft tissue was performed as previously described.[21] The intensity of K_i-67 staining was measured using a scale (0 = no expression, 1 = weak expression, 2 = moderate expression, and 3 = strong expression) and quantified as weighted index (WI = % positive staining in tumor × intensity score). An average of the 10 readings was used for statistical analysis.

For the TUNEL assay, the total cell number and the positive cell number in the same area were counted for five random areas; the result was presented as an average ratio of positive cell number out of total cell number.

Statistical Analysis. The statistical significance of treatment was assessed using the Student's *t*-test for the following studies: *in vitro* cytotoxicity assay, cellular uptake, retention, efflux analysis, and the capillary tubule formation study. $p < 0.05$ was considered statistically significant in all analyses. For the *in vivo* antitumor efficacy assay, a log–linear mixed model with random intercept was used to compare the significance of the mean tumor volumes among each group. The statistical significance of treatment on microtubule, angiogenesis, apoptosis, and cell proliferation in xenograft tumor tissues was assessed using the Kruskal–Wallis test (one-way ANOVA). $p < 0.05$ was considered statistically significant.

Acknowledgment. This work was supported by grants (P50CA128613; U01 CA151802) to D.M.S., U54CA119338 to S.N., and Georgia Cancer Coalition Distinguished Scholar Awards to D.M.S., S.N., and Z.C. The authors thank Dr. Jonathan J. Beitler and Dr. Anthea Hammond for critical reading and editing of the manuscript.

Supporting Information Available: This material is available free of charge *via* the Internet at http://pubs.acs.org.

REFERENCES AND NOTES

1. Ling, V.; Charles, F. Kettering Prize. P-Glycoprotein and Resistance to Anticancer Drugs. *Cancer* **1992**, *69*, 2603–2609.
2. Horwitz, S. B.; Cohen, D.; Rao, S.; Ringel, I.; Shen, H. J.; Yang, C. P. Taxol: Mechanisms of Action and Resistance. *J. Natl. Cancer Inst. Monogr.* **1993**, *15*, 55–61.
3. Gottesman, M. M.; Fojo, T.; Bates, S. E. Multidrug Resistance in Cancer: Role of ATP-Dependent Transporters. *Nat. Rev. Cancer* **2002**, *2*, 48–58.
4. Ferry, D. R.; Traunecker, H.; Kerr, D. J. Clinical Trials of P-glycoprotein Reversal in Solid Tumours. *Eur. J. Cancer* **1996**, *32A*, 1070–1081.
5. McDevitt, C. A.; Callaghan, R. How Can We Best Use Structural Information on P-Glycoprotein to Design Inhibitors? *Pharmacol. Ther.* **2007**, *113*, 429–441.
6. Chow, E. K.; Zhang, X. Q.; Chen, M.; Lam, R.; Robinson, E.; Huang, H.; Schaffer, D.; Osawa, E.; Goga, A.; Ho, D. Nanodiamond Therapeutic Delivery Agents Mediate Enhanced Chemoresistant Tumor Treatment. *Sci. Transl. Med.* **2011**, *3*, 1–10.
7. Merkel, T. J.; Desimone, J. M. Dodging Drug-Resistant Cancer with Diamonds. *Sci. Transl. Med.* **2011**, *3*, 73ps8.
8. Davis, M. E.; Chen, Z. G.; Shin, D. M. Nanoparticle Therapeutics: an Emerging Treatment Modality for Cancer. *Nat. Rev. Drug Discovery* **2008**, *7*, 771–782.
9. MacDiarmid, J. A.; Amaro-Mugridge, N. B.; Madrid-Weiss, J.; Sedliarou, I.; Wetzel, S.; Kochar, K.; Brahmbhatt, V. N.; Phillips, L.; Pattison, S. T.; Petti, C.; *et al.* Sequential Treatment of Drug-Resistant Tumors with Targeted Minicells Containing siRNA or a Cytotoxic Drug. *Nat. Biotechnol.* **2009**, *27*, 643–651.
10. Liu, Z.; Chen, K.; Davis, C.; Sherlock, S.; Cao, Q.; Chen, X.; Dai, H. Drug Delivery with Carbon Nanotubes for *in Vivo* Cancer Treatment. *Cancer Res.* **2008**, *68*, 6652–6660.
11. Noble, C. O.; Kirpotin, D. B.; Hayes, M. E.; Mamot, C.; Hong, K.; Park, J. W.; Benz, C. C.; Marks, J. D.; Drummond, D. C. Development of Ligand-Targeted Liposomes for Cancer Therapy. *Expert. Opin. Ther. Targets* **2004**, *8*, 335–353.
12. Northfelt, D. W.; Martin, F. J.; Working, P.; Volberding, P. A.; Russell, J.; Newman, M.; Amantea, M. A.; Kaplan, L. D. Doxorubicin Encapsulated in Liposomes Containing Surface-Bound Polyethylene Glycol: Pharmacokinetics, Tumor Localization, and Safety in Patients with AIDS-Related Kaposi's Sarcoma. *J. Clin. Pharmacol.* **1996**, *36*, 55–63.
13. Thiery, J. P.; Sleeman, J. P. Complex Networks Orchestrate Epithelial-Mesenchymal Transitions. *Nat. Rev. Mol. Cell Biol.* **2006**, *7*, 131–142.
14. Wang, X.; Yang, L.; Chen, Z. G.; Shin, D. M. Application of Nanotechnology in Cancer Therapy and Imaging. *CA Cancer J. Clin.* **2008**, *58*, 97–110.
15. Farokhzad, O. C.; Cheng, J.; Teply, B. A.; Sherifi, I.; Jon, S.; Kantoff, P. W.; Richie, J. P.; Langer, R. Targeted Nanoparticle-Aptamer Bioconjugates for Cancer Chemotherapy *in Vivo*. *Proc. Natl. Acad. Sci. U. S. A.* **2006**, *103*, 6315–6320.

16. Gu, F.; Zhang, L.; Teply, B. A.; Mann, N.; Wang, A.; Radovic-Moreno, A. F.; Langer, R.; Farokhzad, O. C. Precise Engineering of Targeted Nanoparticles by Using Self-Assembled Biointegrated Block Copolymers. *Proc. Natl. Acad. Sci. U. S. A.* **2008**, *105*, 2586–2591.
17. Wong, H. L.; Rauth, A. M.; Bendayan, R.; Manias, J. L.; Ramaswamy, M.; Liu, Z.; Erhan, S. Z.; Wu, X. Y. A New Polymer-Lipid Hybrid Nanoparticle System Increases Cytotoxicity of Doxorubicin Against Multidrug-Resistant Human Breast Cancer Cells. *Pharm. Res.* **2006**, *23*, 1574–1585.
18. Shaik, N.; Pan, G.; Elmquist, W. F. Interactions of Pluronic Block Copolymers on P-gp Efflux Activity: Experience with HIV-1 Protease Inhibitors. *J. Pharm. Sci.* **2008**, *97*, 5421–5433.
19. Minko, T.; Kopeckova, P.; Pozharov, V.; Kopecek, J. HPMA Copolymer Bound Adriamycin Overcomes MDR1 Gene Encoded Resistance in a Human Ovarian Carcinoma Cell Line. *J. Controlled Release* **1998**, *54*, 223–233.
20. Minko, T.; Kopeckova, P.; Kopecek, J. Preliminary Evaluation of Caspases-Dependent Apoptosis Signaling Pathways of Free and HPMA Copolymer-Bound Doxorubicin in Human Ovarian Carcinoma Cells. *J. Controlled Release* **2001**, *71*, 227–237.
21. Wang, X.; Li, J.; Wang, Y.; Cho, K. J.; Kim, G.; Gjyrezi, A.; Koenig, L.; Giannakakou, P.; Shin, H. J.; Tighiouart, M.; *et al*. HFT-T, a Targeting Nanoparticle, Enhances Specific Delivery of Paclitaxel to Folate Receptor-Positive Tumors. *ACS Nano* **2009**, *3*, 3165–3174.
22. Horio, M.; Lovelace, E.; Pastan, I.; Gottesman, M. M. Agents which Reverse Multidrug-Resistance are Inhibitors of [3H]Vinblastine Transport by Isolated Vesicles. *Biochim. Biophys. Acta* **1991**, *1061*, 106–110.
23. Sivapackiam, J.; Harpstrite, S. E.; Prior, J. L.; Gu, H.; Rath, N. P.; Sharma, V. Synthesis, Molecular Structure, and Validation of Metalloprobes for Assessment of MDR1 P-glycoprotein-Mediated Functional Transport. *Dalton Trans. 39*, 5842−5850.
24. Meister, B.; Kropshofer, G.; Klein-Franke, A.; Strasak, A. M.; Hager, J.; Streif, W. Comparison of Low-Molecular-Weight Heparin and Antithrombin Versus Antithrombin Alone for the Prevention of Symptomatic Venous Thromboembolism in Children with Acute Lymphoblastic Leukemia. *Pediatr. Blood Cancer* **2008**, *50*, 298–303.
25. Icli, F.; Akbulut, H.; Utkan, G.; Yalcin, B.; Dincol, D.; Isikdogan, A.; Demirkazik, A.; Onur, H.; Cay, F.; Buyukcelik, A. Low Molecular Weight Heparin (LMWH) Increases the Efficacy of Cisplatinum Plus Gemcitabine Combination in Advanced Pancreatic Cancer. *J. Surg. Oncol.* **2007**, *95*, 507–512.
26. Presta, M.; Leali, D.; Stabile, H.; Ronca, R.; Camozzi, M.; Coco, L.; Moroni, E.; Liekens, S.; Rusnati, M. Heparin Derivatives as Angiogenesis Inhibitors. *Curr. Pharm. Des.* **2003**, *9*, 553–566.
27. Lee, E.; Kim, Y. S.; Bae, S. M.; Kim, S. K.; Jin, S.; Chung, S. W.; Lee, M.; Moon, H. T.; Jeon, O. C.; Park, R. W.; *et al*. Polyproline-Type Helical-Structured Low-Molecular Weight Heparin (LMWH)-Taurocholate Conjugate as a New Angiogenesis Inhibitor. *Int. J. Cancer* **2009**, *124*, 2755–2765.
28. Collen, A.; Smorenburg, S. M.; Peters, E.; Lupu, F.; Koolwijk, P.; Van Noorden, C.; van Hinsbergh, V. W. Unfractionated and Low Molecular Weight Heparin Affect Fibrin Structure and Angiogenesis in Vitro. *Cancer Res.* **2000**, *60*, 6196–6200.
29. Vlodavsky, I.; Friedmann, Y.; Elkin, M.; Aingorn, H.; Atzmon, R.; Ishai-Michaeli, R.; Bitan, M.; Pappo, O.; Peretz, T.; Michal, I.; *et al*. Mammalian Heparanase: Gene Cloning, Expression and Function in Tumor Progression and Metastasis. *Nat. Med.* **1999**, *5*, 793–802.
30. Freeman, C.; Browne, A. M.; Parish, C. R. Evidence that Platelet and Tumour Heparanases are Similar Enzymes. *Biochem. J.* **1999**, *342*, 361–368.
31. Kirpotin, D. B.; Drummond, D. C.; Shao, Y.; Shalaby, M. R.; Hong, K.; Nielsen, U. B.; Marks, J. D.; Benz, C. C.; Park, J. W. Antibody Targeting of Long-Circulating Lipidic Nanoparticles Does not Increase Tumor Localization but Does Increase Internalization in Animal Models. *Cancer Res.* **2006**, *66*, 6732–6740.
32. Konner, J. A.; Bell-McGuinn, K. M.; Sabbatini, P.; Hensley, M. L.; Tew, W. P.; Pandit-Taskar, N.; Vander Els, N.; Phillips, M. D.; Schweizer, C.; Weil, S. C.; *et al*. Farletuzumab, a Humanized Monoclonal Antibody Against Folate Receptor Alpha, in Epithelial Ovarian Cancer: a Phase I Study. *Clin. Cancer Res.* **2010**, *16*, 5288–5295.
33. Garin-Chesa, P.; Campbell, I.; Saigo, P. E.; Lewis, J. L., Jr.; Old, L. J.; Rettig, W. J. Trophoblast and Ovarian Cancer Antigen LK26. Sensitivity and Specificity in Immunopathology and Molecular Identification as a Folate-Binding Protein. *Am. J. Pathol.* **1993**, *142*, 557–567.
34. Lu, W.; Zhang, G.; Zhang, R.; Flores, L. G., 2nd; Huang, Q.; Gelovani, J. G.; Li, C. Tumor Site-Specific Silencing of NF-KappaB p65 by Targeted Hollow Gold Nanosphere-Mediated Photothermal Transfection. *Cancer Res.* **2010**, *70*, 3177–3188.
35. Akiyama, S.; Fojo, A.; Hanover, J. A.; Pastan, I.; Gottesman, M. M. Isolation and Genetic Characterization of Human KB Cell Lines Resistant to Multiple Drugs. *Somat. Cell Mol. Genet.* **1985**, *11*, 117–126.
36. Shen, D. W.; Cardarelli, C.; Hwang, J.; Cornwell, M.; Richert, N.; Ishii, S.; Pastan, I.; Gottesman, M. M. Multiple Drug-Resistant Human KB Carcinoma Cells Independently Selected for High-Level Resistance to Colchicine, Adriamycin, or Vinblastine Show Changes in Expression of Specific Proteins. *J. Biol. Chem.* **1986**, *261*, 7762–7770.
37. Liu, S.; Zhou, F.; Hook, M.; Carson, D. D. A heparin-Binding Synthetic Peptide of Heparin/Heparan Sulfate-Interacting Protein Modulates Blood Coagulation Activities. *Proc. Natl. Acad. Sci. U. S. A.* **1997**, *94*, 1739–1744.
38. Lake, A. C.; Vassy, R.; Di Benedetto, M.; Lavigne, D.; Le Visage, C.; Perret, G. Y.; Letourneur, D. Low Molecular Weight Fucoidan Increases VEGF165-Induced Endothelial Cell Migration by Enhancing VEGF165 Binding to VEGFR-2 and NRP1. *J. Biol. Chem.* **2006**, *281*, 37844–37852.
39. Weidner, N.; Carroll, P. R.; Flax, J.; Blumenfeld, W.; Folkman, J. Tumor Angiogenesis Correlates with Metastasis in Invasive Prostate Carcinoma. *Am. J. Pathol.* **1993**, *143*, 401–409.